Progress In Electromagnetics Research B, Vol. 31, 297–321, 2011

RESOLUTION THRESHOLD ANALYSIS OF MUSIC ALGORITHM IN RADAR RANGE IMAGING

X. Gu* and Y. H. Zhang

Center for Space Science and Applied Research, CAS, Beijing 100190, China

Abstract—Super-resolution algorithms used in radar imaging, e.g., MUltiple SIgnal Classification (MUSIC), can help us to get much higher resolution image beyond what is limited by the signal's bandwidth. We focus on MUSIC imaging algorithm in the paper and investigate the uniqueness and effectiveness conditions of the MUSIC algorithm when used in 1-D radar range imaging. Unlike conventional radar resolution analysis, we introduced the concept of resolution threshold from Direction of Arrival (DOA) into the MUSIC radar range imaging, we derive an approximate expression of theoretical resolution threshold for 1-D MUSIC imaging algorithm through the approach of asymptotic and statistical analysis to the null spectrum based on the perturbation theory of algebra and matrix theories. Monte Carlo simulations are presented to verify the work.

1. INTRODUCTION

High-resolution radar range imaging has long been a highly focused technique in radar community, which has been widely used in both military and civil applications [1–3]. Usually, high-resolution means large bandwidth is required; however large bandwidth usually leads to high complexity of radar system, not only for hardware but also for imaging processing. In this regard, super-resolution algorithms are preferred choices for realizing high-resolution image without large or ultra-large bandwidth. In deed, spectrum estimation methods, such as MUltiple SIgnal Classification (MUSIC) [4–6] and Estimation of Signal Parameters via Rotational Invariance Techniques (ESPRIT) [7–9], have already been used in realizing super-resolution radar image.

In this paper, we only pay attention to MUSIC. Researches on MUSIC can be traced back to 1979, which was proposed by Schmidt

Received 8 April 2011, Accepted 20 June 2011, Scheduled 26 June 2011

* Corresponding author: Xiang Gu (guxiang@nmrs.ac.cn).

originally for Direction of Arrival (DOA) estimation with incoherent waves [10, 11]. Ever since the MUSIC was proposed, continuous researches have been conducted in the following thirty years [12–23]. As research on the MUSIC goes deeper and deeper, its inherent drawbacks, i.e., huge computation burden as well as weak stability, become a major difficulty in its practical application. Fortunately, a lot of efforts on improving the MUSIC have been made by many researchers. Barabell [24], Rao [25], Krim [26], et al. proposed a Root-MUSIC algorithm to save computation time. Shan [27], Haber [28] et al. discussed the coherent signal in DOA estimation and proposed some practical solutions, such as Spatial Smoothing Process (SSP) [29, 30]. Li [31], Ferreol [32] et al. studied the performance of the MUSIC with the presence of model error or system error. Kaveh [33, 34], Choi [35] et al. studied the statistical performance of the MUSIC and the asymptotic distribution of the null spectrum. Messer [36], Friedlander [37] and et al. extended the MUSIC to non-linear array, such as circular array, or even arbitrary array geometry. Gardner [38], Stoica [39], Yu [40] et al. compared the MUSIC with other algorithms. Yeh [41], Mathews [42], Wang [43] and et al. extended the MUSIC to 2-D DOA. Wang [44] et al. used the high-order MUSIC to improve estimation accuracy. Lei [45], Chiang [46] et al. applied the MUSIC in the communication field.

Moreover, Odendaal et al. firstly reported their work on applying the MUSIC algorithm in radar imaging in 1994 [4], much higher resolution 2-D Inverse Synthetic Aperture Radar (ISAR) images were obtained comparing to the results based on Fast Fourier Transform (FFT). Since then, many researches on the MUSIC in radar imaging have been carried out. Li et al. [47] applied the MUSIC to 3-D target feature extraction via INterferometric SAR (INSAR). Kim et al. [48, 49] applied the MUSIC to the radar target identification as well as to 2-D ISAR with full-polarization technique. Miwa [50] studied the super-resolution imaging for point reflectors near transmitting and receiving array. Quinquis et al. [51] applied the MUSIC and ESPRIT algorithm to the experimental data. In recent years, much more works on the MUSIC in radar imaging have been conducted [5, 6, 52–60], but few of them concern about the resolution issue, which is very important for radar imaging. In this paper, we introduce the concept of resolution threshold from DOA into the MUSIC radar range imaging, and then derive an approximate expression of theoretical resolution threshold. As far as we know, there is no similar study reported yet.

The aim of this paper is to investigate the resolution threshold of the MUSIC algorithm when used in 1-D radar range imaging. Different from the conventional radar resolution definition, we firstly

introduce the concept of resolution threshold from DOA into radar range imaging, and determine whether two adjacent targets could be distinguished by analyzing the null spectrum [33]. We analyze the uniqueness and effectiveness conditions of the MUSIC algorithm, which means that when both of them are simultaneously met then one can get the correct radar image. Based on the asymptotic statistical analyzing approach to the null spectrum with the help of perturbation theory of algebra and matrix theories, an approximate expression of theoretical resolution threshold for 1-D MUSIC algorithm is derived. Monte Carlo simulations are presented to verify the analysis.

The remainder of the paper is organized as follows. We set up radar echo model in range in Section 2, and then we investigate the uniqueness and effectiveness conditions for the MUSIC in Section 3. In Section 4, we analyze the statistical characteristics of the null spectrum, and then derive the expression describing the resolution threshold, and in Section 5, we give some simulations. Finally, we conclude the paper in Section 6.

2. MUSIC ALGORITHM FOR RADAR RANGE IMAGING

We consider the 1-D radar range imaging. As shown in Fig. 1, the number of the scattering centres is K, the sampled frequencies are $f_m = f_0 + m\Delta f$ $(m = 0, \ldots, M-1)$, the distance from the radar antenna to the centre of the imaging zone is R_0, and the coordinates of the scattering centres are d_k $(k = 1, 2, \ldots, K)$, the radar echo can be expressed as

$$x_m = \sum_{k=1}^{K} s_k \cdot e^{-j\frac{4\pi f_m}{c} d_k} + n_m \tag{1}$$

where s_k $(k = 1, 2, \ldots, K)$ denote the reflection coefficients of scatters, which are assumed to be constants in frequency range $f_0 \sim f_{M-1}$, c is the speed of electromagnetic wave in free-space, and n_m denote

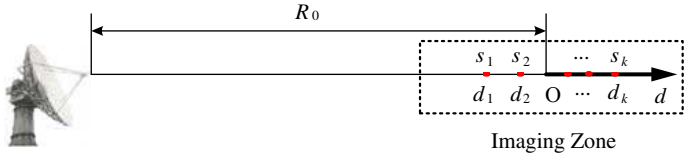

Figure 1. Geometry of radar range imaging.

additive complex white Gaussian noise with zero mean and variance σ^2.

By using vector notation, (1) can be rewritten as follows,

$$\mathbf{X} = \mathbf{AS} + \mathbf{N} \tag{2}$$

$$\mathbf{X} = [x_0, x_1, \ldots, x_{M-1}]^{\mathbf{T}} \tag{3}$$

$$\mathbf{S} = [s_1, s_2, \ldots, s_K]^{\mathbf{T}} \tag{4}$$

$$\mathbf{N} = [n_0, n_1, \ldots, n_{M-1}]^{\mathbf{T}} \tag{5}$$

$$\mathbf{A} = [\mathbf{a}(d_1), \mathbf{a}(d_2), \ldots, \mathbf{a}(d_K)] \tag{6}$$

$$\mathbf{a}(d_k) = \left[e^{-j\frac{4\pi f_0}{c}d_k}, e^{-j\frac{4\pi f_1}{c}d_k}, \ldots, e^{-j\frac{4\pi f_{M-1}}{c}d_k}\right]^{\mathbf{T}} \tag{7}$$

where $\mathbf{T}$ denotes transpose, and $\mathbf{a}(d_K)$ is called the mode vector.

The autocorrelation matrix of the radar echo is defined as,

$$\mathbf{R_X} = \mathbf{XX^H} = \mathbf{ASS^H A^H} + \mathbf{NN^H} \tag{8}$$

where $\mathbf{H}$ denotes complex conjugate transpose.

Different from DOA case, only one set of observation data ("one snapshot") can be obtained in radar range imaging. In other words, the scattered signals from various scattering centres are "coherent", and this "coherence" makes the rank of $\mathbf{R_X}$ is less than K, and in fact the rank of $\mathbf{R_X}$ is equal to 1. The SSP has been demonstrated to be a very effective de-correlating method used in DOA, and it is introduced to the radar range processing. In the following, a brief introduction to SSP is in order.

Let's set up a $p \times 1\,(p > K)$ vector, as illustrated in Fig. 2, the radar echo of M samples can be segmented into $L\,(L = M + 1 - p)$ vectors, if we use $\mathbf{X}_p(l)$ to represent the l-th vector, and then $\mathbf{X}_p(l)$ can be written as

$$\mathbf{X}_p(l) = [x_{l-1}, x_l, \ldots, x_{l+p-2}]^{\mathbf{T}} \tag{9}$$

where $K \le p \le M$ and $1 \le l \le M + 1 - K$.

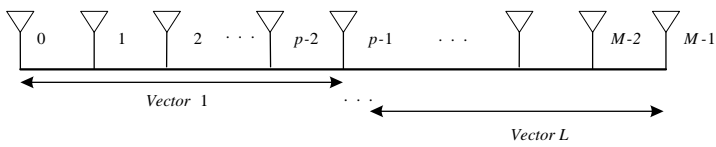

Figure 2. Diagram of Spatial Smoothing Process (SSP).

Equation (9) can be expanded as

$$\begin{aligned}
&\mathbf{X}_p(l) \\
&= \frac{1}{\sqrt{p}} \begin{bmatrix} 1 & 1 & \cdots & 1 \\ e^{-j\frac{4\pi}{c}\Delta f d_1} & e^{-j\frac{4\pi}{c}\Delta f d_2} & & e^{-j\frac{4\pi}{c}\Delta f d_K} \\ \vdots & & \ddots & \vdots \\ e^{-j\frac{4\pi}{c}(p-1)\Delta f d_1} & e^{-j\frac{4\pi}{c}(p-1)\Delta f d_2} & \cdots & e^{-j\frac{4\pi}{c}(p-1)\Delta f d_K} \end{bmatrix} \\
&\sqrt{p} \begin{bmatrix} s_1 e^{-j\frac{4\pi}{c} f_{l-1} d_1} \\ \vdots \\ s_K e^{-j\frac{4\pi}{c} f_{l-1} d_K} \end{bmatrix} + \begin{bmatrix} n_{l-1} \\ n_l \\ \vdots \\ n_{l+p-2} \end{bmatrix}
\end{aligned} \tag{10}$$

Using vector notation, (10) can be rewritten as

$$\mathbf{X}_p(l) = \mathbf{A}_p \mathbf{S}_p(l) + \mathbf{N}_p(l) \tag{11}$$

where

$$\begin{aligned}
\mathbf{S}_p(l) &= \sqrt{p} \left[s_1 e^{-j\frac{4\pi}{c} f_{l-1} d_1}, s_2 e^{-j\frac{4\pi}{c} f_{l-1} d_2}, \quad \ldots, \quad s_K e^{-j\frac{4\pi}{c} f_{l-1} d_K} \right]^{\mathbf{T}} \\
\mathbf{N}_p(l) &= [n_{l-1}, n_l, \ldots, n_{l+p-2}]^{\mathbf{T}} \\
\mathbf{A}_p &= [\mathbf{a}_p(d_1), \mathbf{a}_p(d_2), \ldots, \mathbf{a}_p(d_K)] \\
\mathbf{a}_p(d_k) &= \frac{1}{\sqrt{p}} \left[1, e^{-j\frac{4\pi}{c}\Delta f d_k}, \ldots, e^{-j\frac{4\pi}{c}(p-1)\Delta f d_k} \right]^{\mathbf{T}}
\end{aligned}$$

$\mathbf{a}_p(d_k)$ are called the mode vectors after SSP, $\sqrt{p}$ and $1/\sqrt{p}$ are used for normalization.

To apply the MUSIC algorithm to radar range imaging, we need to follow below three assumptions:

Assumption (1): The mode vectors $\mathbf{a}_p(d_k)$ $(k = 1, 2, \ldots, K)$ are linear independent, and $\mathbf{A}_p$ is fully ranked in column.

Assumption (2): Each element of the addition noise vector $\mathbf{N}$ is complex white Gaussian noise with zero mean and variance σ^2, and it means $\mathbf{E}[\mathbf{N}_p \mathbf{N}_p^{\mathbf{H}}] = \sigma^2 \mathbf{I}$, $\mathbf{E}[\mathbf{N}_p] = \mathbf{0}$ and $\mathbf{E}[\mathbf{N}_p \mathbf{N}_p^{\mathbf{T}}] = \mathbf{O}$, where $\mathbf{0}$ and $\mathbf{O}$ represent zero vector and zero matrix, respectively, $\mathbf{I}$ represents identity matrix, and $\mathbf{E}[\cdot]$ denotes statistical expectation.

Assumption (3): The matrix $\mathbf{E}[\mathbf{S}_p \mathbf{S}_p^{\mathbf{H}}]$ is non-singular, and $rank\{\mathbf{E}[\mathbf{S}_p \mathbf{S}_p^{\mathbf{H}}]\} = K$.

If the above assumptions are all satisfied, it can be easily proved that, the autocorrelation matrix $\mathbf{R}_{\mathbf{X}p}$ of $\mathbf{X}_p(l)$, which is defined as

$$\mathbf{R}_{\mathbf{X}p} = \mathbf{E}\left[\mathbf{X}_p \mathbf{X}_p^{\mathbf{H}}\right] = \mathbf{A}_p \mathbf{E}\left[\mathbf{S}_p \mathbf{S}_p^{\mathbf{H}}\right] \mathbf{A}_p^{\mathbf{H}} + \sigma^2 \mathbf{I} \tag{12}$$

is a matrix with rank of p. The eigen-decomposition of $\mathbf{R}_{\mathbf{X}p}$ can be conducted as

$$\mathbf{R}_{\mathbf{X}p} = \mathbf{U}\boldsymbol{\Sigma}\mathbf{U}^{\mathbf{H}} \tag{13}$$

where $\boldsymbol{\Sigma} = \mathrm{diag}\left(\lambda_1, \lambda_2, \ldots, \lambda_p\right)$ and $\lambda_1, \lambda_2, \ldots, \lambda_p$ are the eigenvalues of $\mathbf{R}_{\mathbf{X}p}$.

According to **Assumption (1)** and **Assumption (3)**, we have

$$\mathbf{U}^{\mathbf{H}}\left\{\mathbf{A}_p\mathbf{E}\left[\mathbf{S}_p\mathbf{S}_p^{\mathbf{H}}\right]\mathbf{A}_p^{\mathbf{H}}\right\}\mathbf{U} = \mathrm{diag}\left(\mu_1^2, \mu_2^2, \ldots, \mu_K^2, 0, \ldots, 0\right) \tag{14}$$

So the eigenvalues of $\mathbf{R}_{\mathbf{X}p}$ can be given by

$$\lambda_i = \begin{cases} \mu_i^2 + \sigma^2 & i = 1, 2, \ldots, K \\ \sigma^2 & i = K+1, K+2, \ldots, p \end{cases} \tag{15}$$

Let's define signal eigenvectors and noise eigenvectors as $\mathbf{U_S}$ and $\mathbf{U_N}$, respectively, as shown in Equations (16)–(18),

$$\mathbf{U_S} = [u_1, u_2, \ldots, u_K] \tag{16}$$

$$\mathbf{U_N} = [u_{K+1}, u_{K+2}, \ldots, u_p] \tag{17}$$

$$\mathbf{U} = \left[\mathbf{U_S} \vdots \mathbf{U_N}\right] \tag{18}$$

In the next, we analyze the $\mathbf{R}_{\mathbf{X}p}\mathbf{U_N}$ as shown by (19) and (20)

$$\mathbf{R}_{\mathbf{X}p}\mathbf{U_N} = [\mathbf{U_S}\mathbf{U_N}]\,\boldsymbol{\Sigma}\begin{bmatrix}\mathbf{U_S^H}\\ \mathbf{U_N^H}\end{bmatrix}\mathbf{U_N} = [\mathbf{U_S}\mathbf{U_N}]\,\boldsymbol{\Sigma}\begin{bmatrix}\mathbf{O}\\ \mathbf{I}\end{bmatrix} = \sigma^2\mathbf{U_N} \tag{19}$$

$$\mathbf{R}_{\mathbf{X}p}\mathbf{U_N} = \mathbf{A}_p\mathbf{E}\left[\mathbf{S}_p\mathbf{S}_p^{\mathbf{H}}\right]\mathbf{A}_p^{\mathbf{H}}\mathbf{U_N} + \sigma^2\mathbf{U_N} \tag{20}$$

Using (19) and (20)

$$\mathbf{A}_p^{\mathbf{H}}\mathbf{U_N} = \mathbf{O} \tag{21}$$

Let's define spatial spectrum as

$$P\left(d\right) = \frac{1}{\mathbf{a}_p\left(d\right)^{\mathbf{H}}\mathbf{U_N}\mathbf{U_N^H}\mathbf{a}_p\left(d\right)} \tag{22}$$

where $\mathbf{a}_p(d)$ is named as the searching vector.

According to [26], in Root-MUSIC algorithm, the roots satisfying Equation (21) give peaks in the spatial spectrum given in (22).

The spatial spectrum can also be defined as

$$P\left(d\right) = \frac{\mathbf{a}_p\left(d\right)^{\mathbf{H}}\mathbf{a}_p\left(d\right)}{\mathbf{a}_p\left(d\right)^{\mathbf{H}}\mathbf{U_N}\mathbf{U_N^H}\mathbf{a}_p\left(d\right)} \tag{23}$$

The distance of each scattering centre can be estimated by searching the peak position of the spatial spectrum function. However the amplitude of each peak contains no information with regard to

the scattering intensities of the scattering centres. Therefore, having estimated d_k $(k = 1, 2, \ldots, K)$, we then construct matrix $\mathbf{A}$ and use the Least Square Method (LSM) to estimate the reflection coefficient of each scattering centre as following

$$\mathbf{S} = \left(\mathbf{A^H A}\right)^{-1} \mathbf{A^H X} \tag{24}$$

3. UNIQUENESS AND EFFECTIVENESS CONDITIONS FOR MUSIC

Among the three assumptions discussed in Section 2, **Assumption (2)** is usually easy satisfied, but **Assumption (1)** and **Assumption (3)** are not.

3.1. Uniqueness Condition Analysis

As we known, $\mathbf{a}_p(d + kc/2\Delta f) = \mathbf{a}_p(d)\,(k = \pm 1, \pm 2, \ldots)$ exists in mathematics, and it is described as "range ambiguity" in radar range imaging. Here, the range ambiguity means that we can get peaks not only in position d, but also in $d + kc/2\Delta f\,(k = \pm 1, \pm 2, \ldots)$, so "artifacts" appears in range profile. In DOA case, the angle of incidence is range from 0° to 360° (or -180° to 180°), so **Assumption (1)** is satisfied naturally.

In order to get a unique range profile of scattering centres, and make the **Assumption (1)** satisfied, the following condition should be met,

$$0 < \frac{4\pi}{c}\Delta f\,(d_{\max} - d_{\min}) \leq 2\pi \tag{25}$$

where $d_{\max}$ and $d_{\min}$ are the maximum and minimum coordinates of the scattering centres.

Equation (25) also means that the frequency step Δf should satisfy

$$\Delta f \leq \frac{c}{2\Delta d_{\max}} \tag{26}$$

where $\Delta d_{\max} = d_{\max} - d_{\min}$ is the maximum dimension of the target.

Equation (25) is called the uniqueness condition, because "range ambiguity" and "artifacts" appears if Equation (25) is unsatisfied.

3.2. Effectiveness Condition Analysis

Let's define

$$\psi = \mathbf{E}\left[\mathbf{S}_p\mathbf{S}_p^{\mathbf{H}}\right] = \frac{1}{L}\sum_{l=1}^{L}\mathbf{S}_p\,(l)\,\mathbf{S}_p^{\mathbf{H}}\,(l) \tag{27}$$

Then, the element of ψ can be computed by

$$\psi(i,j) = \begin{cases} p|s_i|^2 & (i=j) \\ \frac{ps_i s_j^* e^{-j\frac{4\pi}{c}f_0\Delta d_{ij}}}{L} \sum_{l=1}^{L} e^{-j\frac{4\pi}{c}(l-1)\Delta f\,\Delta d_{ij}} & (i\neq j) \end{cases} \tag{28}$$

where $\Delta d_{ij} = d_i - d_j$ and $*$ denotes complex conjugate.

Here, we discuss $\psi(i,j)$ when $i \neq j$, and for convenience, let's set $\tau_{ij} = 2\pi\Delta f\Delta d_{ij}/c$,

$$\psi(i,j) = \begin{cases} ps_i s_j^* e^{-j\frac{4\pi}{c}f_0\Delta d_{ij}} & \tau_{ij} = k\pi\ (k=0,\pm1,\ldots) \\ \frac{ps_i s_j^* e^{-j\frac{4\pi}{c}f_0\Delta d_{ij}} e^{-j(L-1)\tau_{ij}}}{L}\frac{\sin(L\tau_{ij})}{\sin(\tau_{ij})} & \tau_{ij} \neq k\pi\ (k=0,\pm1,\ldots) \end{cases} \tag{29}$$

Assuming L is infinite (usually L is very large), when $\tau_{ij} = k\pi\ (k=0,\pm1,\ldots)$, we have

$$\psi(i,j) = \begin{cases} p|s_i|^2 & (i=j) \\ ps_i s_j^* e^{-j\frac{4\pi}{c}f_0\Delta d_{ij}} & (i\neq j) \end{cases} \tag{30}$$

so the rank of ψ is equal to 1, and **Assumption (3)** is unsatisfied. In this situation, the SSP does not work, and the "coherence" is not de-correlated.

When $\tau_{ij} \neq k\pi\ (k=0,\pm1,\ldots)$, $\frac{ps_i s_j^* e^{-j\frac{4\pi}{c}f_0\Delta d_{ij}} e^{-j(L-1t)\tau_{ij}}}{L}\frac{\sin(L\tau_{ij})}{\sin(\tau_{ij})} \to 0$ when L is infinite (usually L is very large), so we have

$$\psi(i,j) = \begin{cases} p|s_i|^2 & (i=j) \\ 0 & (i\neq j) \end{cases} \tag{31}$$

so ψ is a full-rank diagonal matrix, and **Assumption (3)** is satisfied. Here, the SSP works, and the "coherence" is effective de-correlated.

According to the above analysis, the effectiveness condition of the MUSIC, which makes **Assumption (3)** satisfied, can be concluded as,

$$\tau_{ij} \neq k\pi\ \ (k=0,\pm1,\ldots) \tag{32}$$

Combining (25) and (32),

$$0 < \frac{4\pi}{c}\Delta f\Delta d_{\max} < 2\pi \tag{33}$$

So

$$0 < |\tau_{ij}| < \pi \tag{34}$$

In summary, to effectively apply the MUSIC in radar range imaging and obtain uniquely imaging result, we should guarantee the uniqueness and effectiveness conditions stated as (33).

Theoretically, when L is infinite, the $\psi(i,j)$ $(i \neq j)$ always converge to 0. But in practical situation, L can not be infinite, so the convergence performance of $\psi(i,j)$ $(i \neq j)$ should be considered seriously, especially the convergence rate. Whether $\psi(i,j)(i \neq j)$ is converge to 0 determines the effectiveness of the de-correlating and the convergence rate affects the choice of L, and slow convergence rate requires more sub-vectors. Simulations about the convergence rate of $\psi(i,j)$ $(i \neq j)$ and the choice of L are presented in Section 5.

4. RESOLUTION THRESHOLD FOR MUSIC

In Section 3 we have investigated the uniqueness and effectiveness conditions of the MUSIC algorithm when used in 1-D radar range imaging. In this section, we analyze the statistical performance of the resolution threshold for MUSIC algorithm.

In this section, we firstly derive the statistical expression of the null spectrum, and then analyse the performance of the null spectrum, moreover, we derive an approximate expression for the resolution threshold of the MUSIC. In the following analysis, we assume L is large enough and $\psi(i,j)$ $(i \neq j)$ converges to 0.

4.1. Performance of Null Spectrum

In practice, $\mathbf{R}_{\mathbf{X}p}$ is computed as follows,

$$\tilde{\mathbf{R}}_{\mathbf{X}p} = \frac{1}{L}\sum_{l=1}^{L} \mathbf{X}_p(l)\,\mathbf{X}_p^{\mathbf{H}}(l) = \mathbf{A}_p\left[\frac{1}{L}\sum_{l=1}^{L}\mathbf{S}_p(l)\,\mathbf{S}_p^{\mathbf{H}}(l)\right]\mathbf{A}_p^{\mathbf{H}} + \sigma^2\mathbf{I} \quad (35)$$

where L is finite, and $\tilde{\mathbf{R}}_{\mathbf{X}p}$ is a biased estimation of $\mathbf{R}_{\mathbf{X}p}$.

Let's set the K principal eigenvalues and their eigenvectors of $\tilde{\mathbf{R}}_{\mathbf{X}p}$ as follows

$$\tilde{\lambda}_i = \lambda_i + \beta_i \quad (36)$$

$$\tilde{\mathbf{u}}_i = \mathbf{u}_i + \eta_i \quad (37)$$

where λ_i and $\mathbf{u}_i (i = 1, 2, \ldots, K)$ are the K principal eigenvalues and eigenvectors of $\mathbf{R}_{\mathbf{X}p}$, respectively.

According to literature [61, 62], η_i have the following statistical properties

$$\mathbf{E}\left[\eta_i\eta_j^{\mathbf{H}}\right] \simeq \frac{\lambda_i}{L}\sum_{\substack{k=1\\k\neq i}}^{p}\frac{\lambda_k}{(\lambda_i-\lambda_k)^2}\mathbf{u}_k\mathbf{u}_k^{\mathbf{H}}\delta_{ij} \quad (38)$$

$$\mathbf{E}\left[\eta_i\right] \simeq -\frac{\lambda_i}{2L}\sum_{\substack{k=1\\k\neq i}}^{p}\frac{\lambda_k}{\left(\lambda_i-\lambda_k\right)^2}\mathbf{u}_i \tag{39}$$

Let's define the "null spectrum" as

$$\tilde{D}\left(d\right)=\mathbf{a}_p\left(d\right)^{\mathbf{H}}\tilde{\mathbf{U}}_{\mathbf{X}p}\tilde{\mathbf{U}}_{\mathbf{X}p}^{\mathbf{H}}\mathbf{a}_p\left(d\right)=1-\mathbf{a}_p\left(d\right)^{\mathbf{H}}\tilde{\mathbf{V}}_{\mathbf{X}p}\tilde{\mathbf{V}}_{\mathbf{X}p}^{\mathbf{H}}\mathbf{a}_p\left(d\right) \tag{40}$$

where $\tilde{\mathbf{U}}_{\mathbf{X}p}$ is a $p\times(p-K)$ matrix, whose columns are the $p-K$ noise eigenvectors of $\tilde{\mathbf{R}}_{\mathbf{X}p}$, and $\tilde{\mathbf{V}}_{\mathbf{X}p}$ is a $p\times K$ matrix, whose columns are the K signal eigenvectors.

By taking the expectation of (40) as following

$$\begin{aligned}\mathbf{E}\left[\tilde{D}\left(d\right)\right] &= 1-\mathbf{a}_p\left(d\right)^{\mathbf{H}}\sum_{i=1}^{K}\mathbf{u}_i\mathbf{u}_i^{\mathbf{H}}\mathbf{a}_p\left(d\right)-\mathbf{a}_p\left(d\right)^{\mathbf{H}}\mathbf{E}\left[\sum_{i=1}^{K}\eta_i\eta_i^{\mathbf{H}}\right]\mathbf{a}_p\left(d\right)\\ &\quad -2\mathbf{Re}\left[\mathbf{a}_p\left(d\right)^{\mathbf{H}}\left(\sum_{i=1}^{K}\mathbf{u}_i\mathbf{E}\left[\eta_i^{\mathbf{H}}\right]\right)\mathbf{a}_p\left(d\right)\right]\end{aligned} \tag{41}$$

The ideal null spectrum is

$$D\left(d\right)=1-\mathbf{a}_p\left(d\right)^{\mathbf{H}}\sum_{i=1}^{K}\mathbf{u}_i\mathbf{u}_i^{\mathbf{H}}\mathbf{a}_p\left(d\right) \tag{42}$$

where $D(d)=0$ when $d=d_k$, and $D(d)>0$ when $d\neq d_k$. Then (41) can be rewritten as

$$\begin{aligned}&\mathbf{E}\left[\tilde{D}\left(d\right)\right]\\ &\simeq D\left(d\right)-\mathbf{a}_p\left(d\right)^{\mathbf{H}}\left[\sum_{i=1}^{K}\sum_{\substack{j=1\\j\neq i}}^{p}\frac{\lambda_i\lambda_j}{L\left(\lambda_i-\lambda_j\right)^2}\left(\mathbf{u}_j\mathbf{u}_j^{\mathbf{H}}-\mathbf{u}_i\mathbf{u}_i^{\mathbf{H}}\right)\right]\mathbf{a}_p\left(d\right)\end{aligned} \tag{43}$$

To investigate the resolution threshold, we consider $K=2$, then

$$\begin{aligned}&\mathbf{E}\left[\tilde{D}(d)\right]\\ &\simeq D(d)+\sigma^2\mathbf{a}_p\left(d\right)^{\mathbf{H}}\left[\frac{(p-2)\lambda_1}{L\left(\lambda_1-\sigma^2\right)^2}\mathbf{u}_1\mathbf{u}_1^{\mathbf{H}}+\frac{(p-2)\lambda_2}{L(\lambda_2-\sigma^2)^2}\mathbf{u}_2\mathbf{u}_2^{\mathbf{H}}\right]\mathbf{a}_p(d)\end{aligned} \tag{44}$$

Let's set $\bar{\mathbf{R}}_{\mathbf{X}p}=\mathbf{R}_{\mathbf{X}p}-\sigma^2\mathbf{I}$,

$$\begin{aligned}\bar{\mathbf{R}}_{\mathbf{X}p} &= \mathbf{A}_p\mathbf{E}\left[\mathbf{S}_p\mathbf{S}_p^{\mathbf{H}}\right]\mathbf{A}_p^{\mathbf{H}}\\ &= \left[\mathbf{a}_p\left(d_1\right),\mathbf{a}_p\left(d_2\right)\right]\begin{bmatrix}\psi\left(1,1\right) & \psi\left(1,2\right)\\ \psi\left(2,1\right) & \psi\left(2,2\right)\end{bmatrix}\left[\mathbf{a}_p\left(d_1\right),\mathbf{a}_p\left(d_2\right)\right]^{\mathbf{H}}\end{aligned} \tag{45}$$

where $\Delta d_{12} = d_1 - d_2$.

According to literature [33, 61], the two principal eigenvalues of $\bar{\mathbf{R}}_{\mathbf{X}p}$ are given as following

$$\bar{\lambda}_{1(2)} = p\frac{P_1 + P_2 + 2\sqrt{P_1 P_2} \cdot \mathrm{Re}\left(\rho\phi\right)}{2} \left[1 \pm \sqrt{1 - \frac{4P_1 P_2 \left(1 - |\phi|^2\right)\left(1 - |\rho|^2\right)}{\left[P_1 + P_2 + 2\sqrt{P_1 P_2} \cdot \mathrm{Re}\left(\rho\phi\right)\right]^2}}\right] \tag{46}$$

where $P_1 = |s_1|^2$, $P_2 = |s_2|^2$, $\rho = \psi(1,2)/\sqrt{P_1 P_2}$, and $\phi = \mathbf{a}_p(d_1)^{\mathbf{H}}\mathbf{a}_p(d_2)$ is defined as the cosine of the angle between mode vector $\mathbf{a}_p(d_1)$ and $\mathbf{a}_p(d_2)$ in literature [61].

ϕ can be expressed as

$$\phi = \frac{e^{j(p-1)\tau_{12}}}{p}\frac{\sin\left(p\tau_{12}\right)}{\sin\left(\tau_{12}\right)} \quad (0 < |\tau_{12}| < \pi) \tag{47}$$

where $\tau_{12} = 2\pi\Delta f \Delta d_{12}/c$ and $\Delta d_{12} = d_1 - d_2$.

And, according to the uniqueness and effectiveness conditions, and assuming L is large (this is usually true), we can get $\rho = \psi(1,2)/\sqrt{P_1 P_2} \to 0$.

Next, we investigate the null spectrum in case of $\phi = 0$ and $\phi \neq 0$, respectively.

A. $\phi = 0$ ***case***

According to (47),

$$\tau_{12} = \frac{k\pi}{p} \quad (k = \pm 1, \pm 2, \ldots, \pm p - 1) \tag{48}$$

The two principal eigenvalues and eigenvectors of $\mathbf{R}_{\mathbf{X}p}$ are given in (49) and (50),

$$\lambda_{1(2)} = \bar{\lambda}_{1(2)} + \sigma^2 = pP_{1(2)} + \sigma^2 \tag{49}$$

$$\mathbf{u}_{1(2)} = \frac{c_{1(2)}}{\left|c_{1(2)}\right|}\mathbf{a}_p\left(d_{1(2)}\right) \tag{50}$$

where $c_{1(2)}$ are constants, and $P_1 = |s_1|^2$, $P_2 = |s_2|^2$.

By using $D(d_{1(2)}) \equiv 0$, (44) can be expressed as

$$\mathbf{E}\left[\tilde{D}\left(d_{1(2)}\right)\right] = \frac{(p-2)}{pL}\left[\frac{\sigma^2}{P_{1(2)}} + \frac{1}{p}\left(\frac{\sigma^2}{P_{1(2)}}\right)^2\right] \tag{51}$$

Equation (51) states that $\sigma^2/P_{1(2)}$, L and p are the factors influencing the performance of the null spectrum. Signal to Noise Ratio (SNR) can be given

$$\mathrm{SNR} = 10 \cdot \log_{10}\left[(p_1 + p_2)/\sigma^2\right] \tag{52}$$

B. $\phi \neq 0$ ***case***
According to (47), we have

$$\tau_{12} \neq \frac{k\pi}{p}\,(k = \pm 1, \ldots, \pm p - 1) \quad \text{and} \quad 0 < |\tau_{12}| < \pi \tag{53}$$

For convenience, assume $s_1 = s_2$ and $P_1 = P_2 = P$, and the two principal eigenvalues and eigenvectors of $\mathbf{R}_{\mathbf{X}p}$ are expressed as following,

$$\lambda_{1(2)} = \bar{\lambda}_{1(2)} + \sigma^2 = pP\,(1 \pm |\phi|) + \sigma^2 \tag{54}$$

$$\mathbf{u}_{1(2)} = \frac{c_{1(2)}}{\left|c_{1(2)}\right|} \frac{\mathbf{a}_p\,(d_1) \pm \frac{|\phi|}{\phi}\mathbf{a}_p\,(d_2)}{\sqrt{2\,(1 \pm |\phi|)}} \tag{55}$$

where $c_{1(2)}$ are constants.

$$\left|\mathbf{a}_p\left(d_{1(2)}\right)^{\mathbf{H}}\mathbf{u}_1\right|^2 = \frac{\bar{\lambda}_1}{2pP} \tag{56}$$

$$\left|\mathbf{a}_p\left(d_{1(2)}\right)^{\mathbf{H}}\mathbf{u}_2\right|^2 = \frac{\bar{\lambda}_2}{2pP} \tag{57}$$

Then

$$\mathbf{E}\left[\tilde{D}\left(d_{1(2)}\right)\right] = \frac{(p-2)\,\sigma^2}{pLP}\left[1 + \frac{\sigma^2}{pP\left(1 - |\phi|^2\right)}\right] \tag{58}$$

Without loss of generality, we study whether two very close targets can be distinguished and investigate the resolution threshold issue, so the assumption $p\tau_{12} < 1$ does make sense.

According to the series expansion of trigonometric function, $|\phi|^2$ can be formulated,

$$|\phi|^2 = \left[\frac{\sin\left(p\tau_{12}\right)}{p\sin\left(\tau_{12}\right)}\right]^2 \simeq 1 - \frac{1}{3}\left(p\tau_{12}\right)^2 + \frac{2}{45}\left(p\tau_{12}\right)^4 \tag{59}$$

By substituting (59) into (58),

$$\mathbf{E}\left[\tilde{D}\left(d_{1(2)}\right)\right] \simeq \frac{(p-2)\,\sigma^2}{pLP}\left\{1 + \frac{\sigma^2}{pP\left[\left(p\tau_{12}\right)^2/3 - 2/45 \cdot \left(p\tau_{12}\right)^4\right]}\right\} \tag{60}$$

Let's define $B_s = p\Delta f$ as "sub-bandwidth", so

$$\mathbf{E}\left[\tilde{D}\left(d_{1(2)}\right)\right] \simeq \frac{(p-2)}{pL}\left\{\frac{\sigma^2}{P} + \frac{1}{p\cdot\left[(2\pi/c)^2\left(B_s\Delta d_{12}\right)^2/3 - 2/45\cdot(2\pi/c)^4\left(B_s\Delta d_{12}\right)^4\right]}\left(\frac{\sigma^2}{P}\right)^2\right\} \quad (61)$$

Unlike $\phi = 0$ case, the second parts in bracket of (61) are much more complex than that in (51). From (61), it is clear that σ^2/P, L, p, B_s and Δd_{12} are the influencing factors on the spatial null spectrum, but B_s and Δd_{12} have limited impact on $\mathbf{E}[\tilde{D}(d_{1(2)})]$. And the SNR can be expressed,

$$\mathrm{SNR} = 10\cdot\log_{10}\left(2P/\sigma^2\right) \quad (62)$$

4.2. Performance of Resolution Threshold

Quite different from the conventional radar resolution analysis, in this paper, we introduce the concept of resolution threshold of DOA into radar range imaging, and determine whether two adjacent targets could be distinguished by analyzing the null spectrum, i.e., $\mathbf{E}[\tilde{D}(d_1)]$ and $\mathbf{E}[\tilde{D}(d_2)]$ should be both smaller than $\mathbf{E}[\tilde{D}((d_1+d_2)/2)]$ by assuming the two scattering centres have same reflection coefficient [33].

Let's set $d_{12} = (d_1+d_2)/2$, then

$$\begin{aligned}&\mathbf{E}\left[\tilde{D}\left(d_{12}\right)\right]\\ =\ & 1 - \mathbf{a}_p\left(d_{12}\right)^{\mathbf{H}}\left(\mathbf{u}_1\mathbf{u}_1^{\mathbf{H}} + \mathbf{u}_2\mathbf{u}_2^{\mathbf{H}}\right)\mathbf{a}_p\left(d_{12}\right)\\ & +\sigma^2\mathbf{a}_p\left(d_{12}\right)^{\mathbf{H}}\left[\frac{(p-2)\lambda_1}{L\left(\lambda_1-\sigma^2\right)^2}\mathbf{u}_1\mathbf{u}_1^{\mathbf{H}} + \frac{(p-2)\lambda_2}{L\left(\lambda_2-\sigma^2\right)^2}\mathbf{u}_2\mathbf{u}_2^{\mathbf{H}}\right]\mathbf{a}_p\left(d_{12}\right)\end{aligned} \quad (63)$$

Here, we define the resolution threshold

$$\frac{\mathbf{E}\left[\tilde{D}\left(d_1\right)\right] + \mathbf{E}\left[\tilde{D}\left(d_2\right)\right]}{2} \le \mathbf{E}\left[\tilde{D}\left(d_{12}\right)\right] \quad (64)$$

A. $\phi = 0$ ***case***

Using $\phi = \mathbf{a}_p(d_1)^{\mathbf{H}}\mathbf{a}_p(d_2) = 0$ and $\mathbf{u}_{1(2)} = \frac{c_{1(2)}}{|c_{1(2)}|}\mathbf{a}_p(d_{1(2)})$

$$\left|\mathbf{a}_p\left(d_{12}\right)^{\mathbf{H}}\mathbf{u}_1\right| = \left|\mathbf{a}_p\left(d_{12}\right)^{\mathbf{H}}\mathbf{u}_2\right| \quad (65)$$

Let's define $\nabla^2 = |\mathbf{a}(d_{12})^{\mathbf{H}}u_1|^2 = |\mathbf{a}(d_{12})^{\mathbf{H}}u_2|^2$, $\mathbf{E}[\tilde{D}(d_{12})]$ and $\mathbf{E}[\tilde{D}(d_{1(2)})]$ can be calculated,

$$\mathbf{E}\left[\tilde{D}\left(d_{12}\right)\right] \simeq 1 - 2\nabla^2 + \sigma^2\frac{2\left(p-2\right)\lambda}{L\left(\lambda-\sigma^2\right)^2}\nabla^2 \quad (66)$$

$$\mathbf{E}\left[\tilde{D}\left(d_{1(2)}\right)\right] \simeq \sigma^2 \frac{(p-2)\,\lambda}{L\left(\lambda-\sigma^2\right)^2} \tag{67}$$

where $\lambda = \lambda_1 = \lambda_2$.

From (66) and (67), if the following equation is satisfied, the two scattering centres can be distinguished.

$$\left[\frac{(p-2)\lambda\sigma^2}{L\left(\lambda-\sigma^2\right)^2} - 1\right] \cdot \left(2\nabla^2 - 1\right) \geq 0 \tag{68}$$

In (68), $(p-2)\lambda\sigma^2/2L(\lambda-\sigma^2)^2 - 1 < 0$ is always guaranteed, so if $2\nabla^2 - 1 < 0$, the two scattering centres can be distinguished.

Consider

$$\nabla^2 = \frac{1}{p^2}\left[\sin\left(\frac{k\pi}{2}\right) \Big/ \sin\left(\frac{k\pi}{2p}\right)\right]^2 \quad k = \pm 1, \pm 2, \ldots \pm (p-1) \tag{69}$$

(a) when k is an even number, $\nabla^2 = 0$, and $2\nabla^2 - 1 < 0$, the two scattering centres can be distinguished.

(b) when k is an odd number

$$2\nabla^2 - 1 = 2 \Big/ \left[p \sin\left(\frac{k\pi}{2p}\right)\right]^2 - 1 \tag{70}$$

As we known, $p > K = 2$, so $2\nabla^2 - 1 < 0$ is satisfied, and the two scattering centres can be distinguished.

In summary, the two scattering centres are always distinguishable when $\phi = 0$ is satisfied.

B. $\phi \neq 0$ ***case***

According to [33], we have

$$\begin{aligned}\left|\mathbf{a}_p\left(d_{12}\right)^{\mathbf{H}}\mathbf{u}_1\right|^2 &= \frac{1}{2\left(1+|\phi|\right)}\left|\mathbf{a}_p\left(d_{12}\right)^{\mathbf{H}}\left[\mathbf{a}_p\left(d_1\right) + \frac{|\phi|}{\phi}\mathbf{a}_p\left(d_2\right)\right]\right|^2 \\ &= \frac{2}{\left(1+|\phi|\right)}\left[\frac{\sin\left(p\tau_{12}/2\right)}{p\sin\left(\tau_{12}/2\right)}\right]^2 \end{aligned} \tag{71}$$

$$\begin{aligned}\left|\mathbf{a}_p\left(d_{12}\right)^{\mathbf{H}}\mathbf{u}_2\right|^2 &= \frac{1}{2\left(1-|\phi|\right)}\left|\mathbf{a}_p\left(d_{12}\right)^{\mathbf{H}}\left[\mathbf{a}_p\left(d_1\right) - \frac{|\phi|}{\phi}\mathbf{a}_p\left(d_2\right)\right]\right|^2 \\ &\simeq 0 \end{aligned} \tag{72}$$

Let's set $\nabla^2 = |\mathbf{a}_p(d_{12})^{\mathbf{H}}\mathbf{u}_1|^2$,

$$\mathbf{E}\left[\tilde{D}\left(d_{12}\right)\right] \simeq 1 - \nabla^2 + \sigma^2 \frac{(p-2)\,\lambda_1}{L\left(\lambda_1-\sigma^2\right)^2}\nabla^2 \tag{73}$$

By substituting $\lambda_1 = pP(1+|\phi|)+\sigma^2$ into (73),

$$\mathbf{E}\left[\tilde{D}\left(d_{12}\right)\right] \simeq 1-\nabla^2+\sigma^2\frac{(p-2)\left[pP\left(1+|\phi|\right)+\sigma^2\right]}{L\left[pP\left(1+|\phi|\right)\right]^2}\nabla^2 \tag{74}$$

According to the series expansion of trigonometric function,

$$\begin{aligned}&\mathbf{E}\left[\tilde{D}\left(d_{12}\right)\right]\\ \simeq\ &\frac{\left(p\tau_{12}\right)^4}{720}+\frac{(p-2)\,\sigma^2}{pLP}\cdot\left\{\left[\frac{1}{2}+\frac{1}{24}\left(p\tau_{12}\right)^2+\frac{1}{1440}\left(p\tau_{12}\right)^4\right]\right.\\ &\left.+\frac{\sigma^2}{pP}\left[\frac{1}{4}+\frac{1}{24}\left(p\tau_{12}\right)^2+\frac{1}{360}\left(p\tau_{12}\right)^4\right]\right\}\end{aligned} \tag{75}$$

By using the fact of $p\tau_{12}<1$, (60) and (75) can be simplified as (76) and (77),

$$\mathbf{E}\left[\tilde{D}\left(d_{1(2)}\right)\right] \simeq \frac{(p-2)\,\sigma^2}{pLP}\left[1+\frac{3}{p\left(p\tau_{12}\right)^2}\frac{\sigma^2}{P}\right] \tag{76}$$

$$\begin{aligned}\mathbf{E}\left[\tilde{D}\left(d_{12}\right)\right] \simeq\ &\frac{\left(p\tau_{12}\right)^4}{720}+\frac{(p-2)\,\sigma^2}{pLP}\left\{\left[\frac{1}{2}+\frac{1}{24}\left(p\tau_{12}\right)^2\right]\right.\\ &\left.+\frac{1}{p}\left[\frac{1}{4}+\frac{1}{24}\left(p\tau_{12}\right)^2\right]\frac{\sigma^2}{P}\right\}\end{aligned} \tag{77}$$

Simulations about the null spectrum of $\mathbf{E}[\tilde{D}(d_1)]$, $\mathbf{E}[\tilde{D}(d_2)$ and $\mathbf{E}[\tilde{D}((d_1+d_2)/2)]$ are presented in Section 5, and the SNR can be expressed as

$$\mathrm{SNR}=10\cdot\log_{10}\left(2P/\sigma^2\right) \tag{78}$$

According to the definition of resolution threshold as shown in (64), the extreme resolution satisfied

$$\mathbf{E}\left[\tilde{D}\left(d_{1(2)}\right)\right]=\mathbf{E}\left[\tilde{D}\left(d_{12}\right)\right] \tag{79}$$

Using (76) and (77), and assuming $\sigma^2/P<1$ (the assumption is usually true) and $p\tau_{12}<1$,

$$\frac{\left(p\tau_{12}\right)^4}{720}-\frac{(p-2)\sigma^2}{pLP}\left[\frac{1}{2}+\frac{3}{p\left(p\tau_{12}\right)^2}\frac{\sigma^2}{P}\right]=0 \tag{80}$$

(a) when $\frac{3}{p(p\tau_{12})^2}\frac{\sigma^2}{P}\gg\frac{1}{2}$

$$\Delta d_{12}\approx\frac{1}{\pi}\left[\frac{p-2}{p}\frac{2160}{pL}\left(\frac{\sigma^2}{P}\right)^2\right]^{1/6}\frac{c}{2B_s}\quad(\Delta d_{12}>0) \tag{81}$$

(b) when $\frac{3}{p(p\tau_{12})^2}\frac{\sigma^2}{P} \ll \frac{1}{2}$

$$\Delta d_{12} \approx \frac{1}{\pi}\left(\frac{p-2}{p}\frac{360}{L}\frac{\sigma^2}{P}\right)^{1/4}\frac{c}{2B_s} \quad (\Delta d_{12} > 0) \tag{82}$$

(c) when $\frac{3}{p(p\tau_{12})^2}\frac{\sigma^2}{P} \approx \frac{1}{2}$

$$\Delta d_{12} \approx \frac{1}{\pi}\left(\frac{p-2}{p}\frac{720}{L}\frac{\sigma^2}{P}\right)^{1/4}\frac{c}{2B_s} \quad (\Delta d_{12} > 0) \tag{83}$$

The above expression is the resolution threshold of the MUSIC algorithm when used in radar range imaging. From (81) and (83), the resolution threshold is closely relative to p, L, σ^2/P and B_s. And $c/2B_s$ can be regard as the resolution of the sub-bandwidth.

5. SIMULATION RESULTS

In this section, simulations are presented to demonstrate the uniqueness condition, convergence performance of $\psi(i,j)\,(i \neq j)$, performance of null spectrum and resolution threshold.

5.1. Uniqueness Condition Simulation

Simulations about the uniqueness condition are shown in Fig. 3. Two targets are locating at -5.0 m and 5.0 m, their reflection coefficients are 0.90 and 0.80, respectively, the centre frequency of the transmitting signal is 10 GHz (X-band), the sample number in frequency is 50, and the length of sub-vector in SSP is 8. 500 times of Monte Carlo simulations are conducted. According to (26), the frequency step should be less than 15 MHz. Figs. 3(a) and (b) show that range imaging

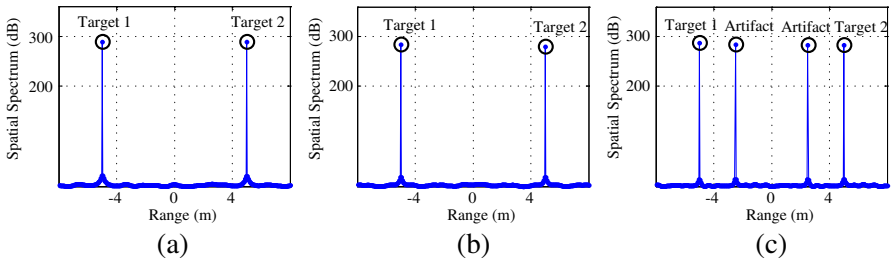

Figure 3. Radar imagery results with frequency step of (a) 10 MHz, (b) 15 MHz and (c) 20 MHz. (In the abscissa, the range profile is just relative, i.e., the distance from radar to the reference point is omitted).

is correctly obtained when frequency step are 10 MHz and 15 MHz, respectively, however when the frequency step is as large as 20 MHz, as shown in Fig. 3(c), "artifacts" appears in range imaging.

5.2. Convergence Performance of $\psi(\mathbf{i},\mathbf{j})$ $(\mathbf{i} \neq \mathbf{j})$

In Section 3, we discussed the convergence performance of $\psi(i,j)$ $(i \neq j)$, especially the convergence rate. Fig. 4(a) shows that the convergence rate is related to the value of $|\tau_{ij}|$. When $|\tau_{ij}|$ is close to $\pi/2$, the convergence rate become fast; when $|\tau_{ij}|$ is close to 0 or π, the convergence rate is slow. Fig. 4(b) shows how to choose an appropriate value of L with different $|\tau_{ij}|\,(0 < |\tau_{ij}| < \pi)$ when $\psi\,(i,j)\,(i \neq j)$ converge to 0.02. And it shows that we can choose $L < 100$ as $\pi/5 \leq |\tau_{ij}| \leq 4\pi/5$, but L increases rapidly when $0 < |\tau_{ij}| < \pi/5$ or $4\pi/5 < |\tau_{ij}| < \pi$, i.e., we should choose $L > 500$ when $|\tau_{ij}|$ is close to 0 or π.

5.3. Performance of Null Spectrum

Simulations of the null spectrum are given in Fig. 5 ($\phi = 0$ case) and Fig. 6 ($\phi \neq 0$ case). In Fig. 5, positions of two targets are -2.5 m and 7.5 m, and their reflection coefficients are 0.90 and 0.80, respectively. The centre frequency of the transmitting signal is 10 GHz, and frequency step is 7.5 MHz, and the number of Monte Carlo test is 500. In Fig. 6, two targets' positions are 0.0 m and 1.0 m, and reflection coefficients are both 0.90. The centre frequency of the transmitting signal is 10 GHz, and frequency step is 0.75 MHz, and the number of

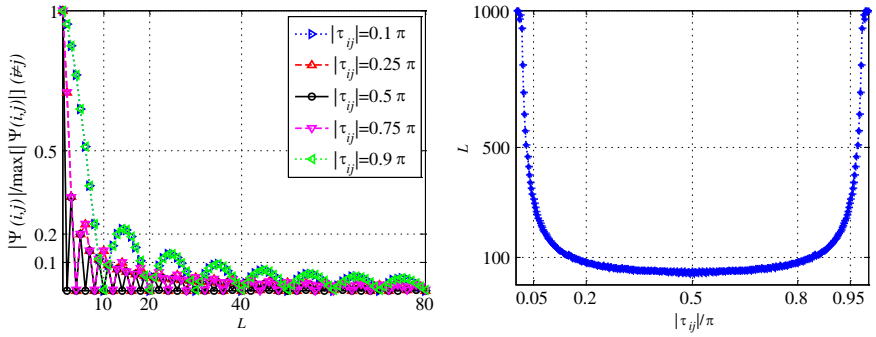

Figure 4. The performance of (a) convergence rate of $\psi\,(i,j)(i \neq j)$ and (b) choice of L with different $|\tau|$.

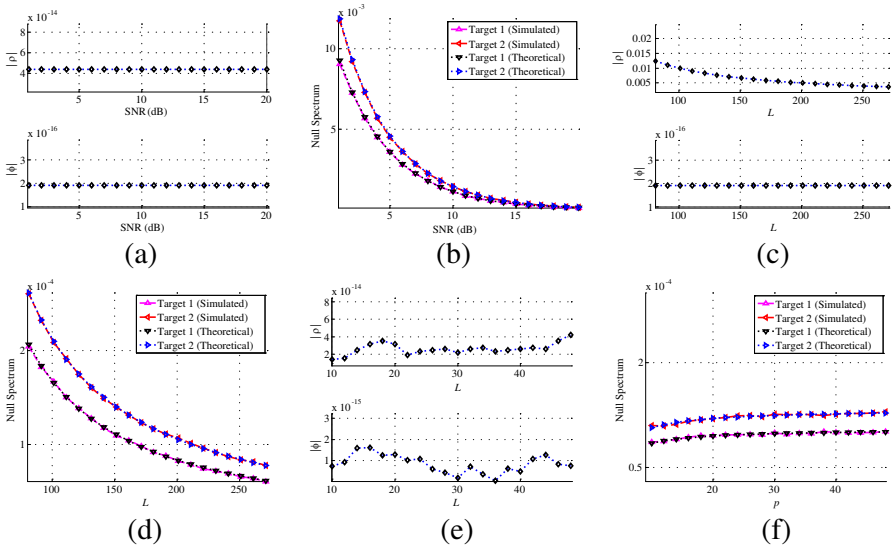

Figure 5. The curves of the null spectrum relative to (a)(b) SNR ($p = 30$, $L = 150$), (c)(d) L ($p = 30$, SNR $= 30\,\text{dB}$) and (e)(f) p ($L = 150$, SNR $= 30\,\text{dB}$) when $\phi = 0$.

Monte Carlo test is 500. In these simulations, L is large enough and $\rho \to 0$. In addition, $p\tau_{12} < 1$ is used when $\phi \neq 0$. The relationships between the null spectrum and SNR, L and p are depicted in Fig. 5 ($\phi = 0$ case) and Fig. 6 ($\phi \neq 0$ case). It is observed that the simulation results are consistent to the theoretical ones [see Formulation (51) and (61)]. In Fig. 5, it shows that null spectrum obviously decreases with the increasing of SNR and L, but has little relationship with p when $p \gg 2$. The reason why target 1's null spectrum is less than target 2 is that its reflection coefficient is greater than that of target 2. In Figs. 5(a) (b), the null spectrum is inverse to L. In Figs. 5(c) (d), the relationship between the null spectrum and SNR is more complex because of the presence of the quadratic term of σ^2/P; and in Figs. 5(e) (f), when $p \gg 2$ and SNR is high, the change of p has little impact on the null spectrum. Fig. 6 shows the similar relationship between the null spectrum and SNR, L and p, the only difference is that the quadratic term of σ^2/P when $\phi \neq 0$ is much more complex, and its null spectrum is also relate to B_s and Δd_{12}.

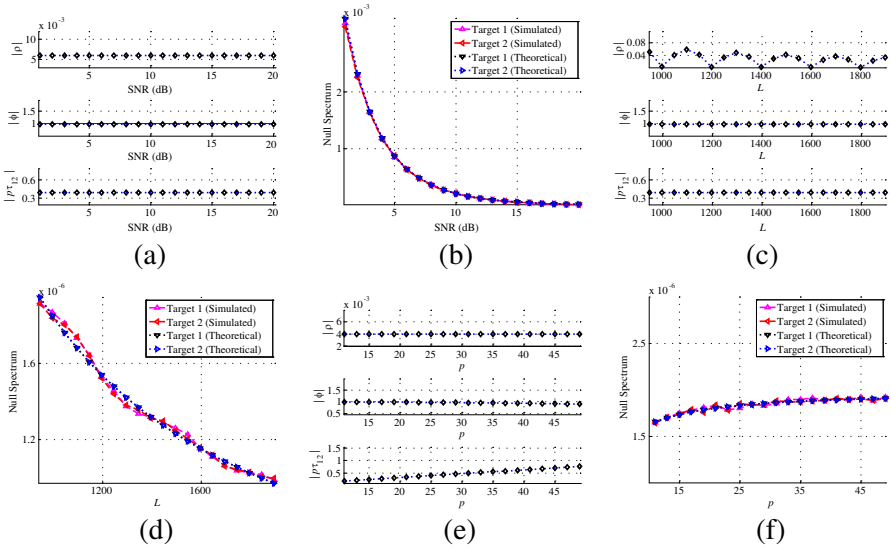

Figure 6. The curves of the null spectrum relative to (a)(b) SNR ($p = 25$, $L = 1000$), (c)(d) L ($p = 25$, SNR $= 30$ dB) and (e)(f) p ($L = 1000$, SNR $= 30$ dB) when $\phi \neq 0$.

5.4. Resolution Threshold of MUSIC ($\phi \neq 0$ Case)

Simulations of the resolution threshold ($\phi \neq 0$ case) are given in Fig. 7. Two targets are locating at -0.05 m and 0.05 m, their reflection coefficients are both 0.90, and the centre frequency is 10 GHz, the frequency step is 15 MHz, and the number of Monte Carlo test is 500. Fig. 7 shows the relationship between the resolution threshold and SNR, L and p. In simulations, $\rho \to 0$ and $\delta_d p < 1$ are satisfied.

In Fig. 7, it shows that the simulation results are consistent to the theoretical ones [see Formulation (76) and (77)]. And in Figs. 7(a) (b), the null spectrum decreases with the increasing of SNR, and the intersection point of the curves means that two targets can be distinguished after this intersection (SNR $= 15$ dB). In Figs. 7(c) (d), the null spectrum also decreases with the increasing of L, and two targets can be distinguished when $L > 500$. In Figs. 7(e) (f), the null spectrum of midpoint changes dramatically with the increasing of p, but the null spectrum of targets are almost unchanged. The intersection point is $p = 15$, it means targets can be distinguished when $p > 15$.

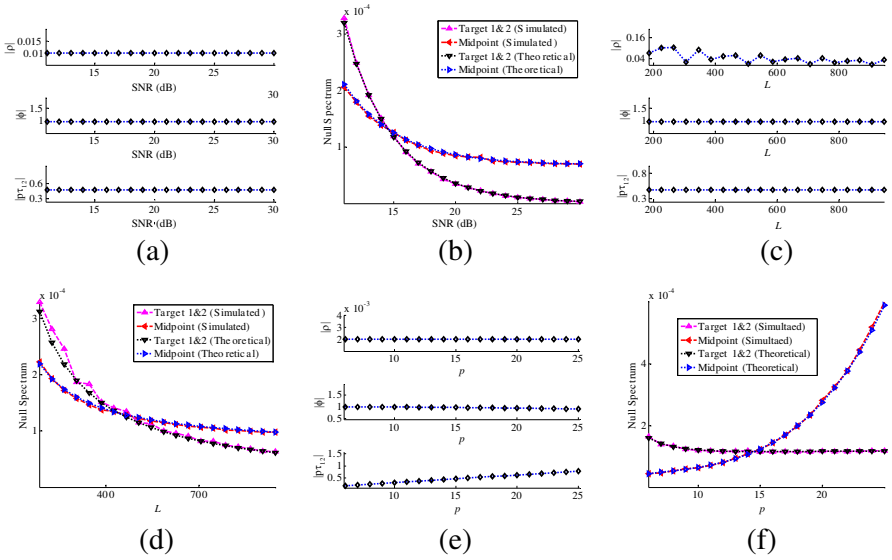

Figure 7. The curves of the resolution threshold relative to (a)(b) SNR ($p = 15$, $L = 500$), (c)(d) L ($p = 15$, SNR $= 20\,\mathrm{dB}$) and (e)(f) p ($L = 500$, SNR $= 15\,\mathrm{dB}$) when $\phi \neq 0$.

6. CONCLUSIONS

The application of the MUSIC algorithm in radar range imaging is discussed in this paper, and the asymptotic statistical analysis of the null spectrum and the resolution threshold is presented, which is closely related to the performance of the MUSIC algorithm. Theoretical expression of the null spectrum is derived firstly. By using its statistic characteristics, we derived the uniqueness and effectiveness conditions for MUSIC, and simulations illustrate that only when the two conditions are met simultaneity can the unique image of targets be obtained; otherwise "artifacts" appears. At last, the expression of the resolution threshold of MUSIC used in radar range imaging is presented based on the asymptotic statistical characteristics of the null spectrum. Monte Carlo tests validate the derivations.

In this paper, we only focus on the performance of the MUSIC algorithm used in radar range profiles, the follow-up work should be the performance of the MUSIC algorithm used in two or three dimension radar imaging.

REFERENCES

1. August, W. R., *Principles of High-Resolution Radar*, Artech House Publishers, Boston, USA, 1996.
2. Son, J. S., G. Thomas, and B. C. Flores, *Range-Doppler Radar Imaging and Motion Compensation*, Artech House Publishers, London, UK, 2001.
3. Hamish, D. M., *Modern Radar Systems*, 2nd edition, Artech House Publishers, Boston, USA, 2008.
4. Odendaal, J. W., E. Barnard, and C. W. I. Pistorius, "Two-dimensional super-resolution radar imaging using the MUSIC algorithm," *IEEE Trans. Antennas Propagat.*, Vol. 42, No. 10, 1386–1391, 1994.
5. Kim, K., D. Seo, and H. Kim, "Efficient radar target recognition using the MUSIC algorithm and invariant features," *IEEE Trans. Antennas Propagat.*, Vol. 50, No. 3, 325–337, 2002.
6. Yoon, Y. and M. G. Amin, "High-resolution through-the-wall radar imaging using beamspace MUSIC," *IEEE Trans. Antennas Propagat.*, Vol. 56, No. 6, 1763–1774, 2008.
7. Roy, R., A. Paulraj, and T. Kailath, "ESPRIT — A subspace rotation approach to estimation of parameters of cisoids in noise," *IEEE Trans. Acoust., Speech, Signal Processing*, Vol. 34, No. 5, 1340–1342, 1986.
8. Roy, R. and T. Kailath, "ESPRIT — Estimation of signal parameters via rotational invariance techniques," *IEEE Trans. Acoust., Speech, Signal Processing*, Vol. 37, No. 7, 984–995, 1989.
9. Rouquette, S. and M. Najim, "Estimation of frequencies and damping factors by two-dimensional ESPRIT type methods," *IEEE Trans. Signal Processing*, Vol. 49, No. 1, 237–245, 2001.
10. Schmidt, R., "Multiple emitter location and signal parameter estimation," *Proc. RADC Spectral Estimation Workshop*, Rome Air Development Center, New York, October 1979.
11. Schmidt, R., "Multiple emitter location and signal parameter estimation," *IEEE Trans. Antennas Propagat.*, Vol. 34, No. 3, 276–280, 1986.
12. Lee, H. B. and M. S. Wengrovitz, "Resolution threshold of beamspace MUSIC for two closely spaced emitters," *IEEE Trans. Acoust., Speech, Signal Processing*, Vol. 38, No. 9, 1545–1559, 1990.
13. Yamada, H., M. Ohmiya, Y. Ogawa, and K. Itoh, "Super-resolution techniques for time-domain measurements with a

network analyzer," *IEEE Trans. Antennas Propagat.*, Vol. 39, No. 2, 177–183, 1991.

14. Li, F., H. Liu, and R. J. Vaccaro, "Performance analysis for DOA estimation algorithms: Unification, simplification, and observations," *IEEE Trans. Aerosp. Electron. Syst.*, Vol. 29, No. 4, 1170–1184, 1993.
15. Cheng, C. and Y. Hua, "Performance analysis of the MUSIC and pencil-MUSIC algorithms for diversely polarized array," *IEEE Trans. Signal Processing*, Vol. 42, No. 11, 3150–3165, 1994.
16. Thompson, J. S., P. M. Grant, and B. Mulgrew, "Performance of spatial smoothing algorithms for correlated sources," *IEEE Trans. Signal Processing*, Vol. 44, No. 4, 1040–1046, 1996.
17. Astely, D. and B. Ottersten, "The effects of local scattering on direction of arrival estimation with MUSIC," *IEEE Trans. Signal Processing*, Vol. 47, No. 12, 3220–3234, 1999.
18. McCloud, M. L. and L. L. Scharf, "A new subspace identification algorithm for high-resolution DOA estimation," *IEEE Trans. Antennas Propagat.*, Vol. 50, No. 10, 1382–1390, 2002.
19. Charge, P., Y. Wang, and J. Saillard, "An extended cyclic MUSIC algorithm," *IEEE Trans. Signal Processing*, Vol. 51, No. 7, 1695–1701, 2003.
20. Kim, J.-T., S.-H. Moon, D. Han, and M.-J. Cho, "Fast DOA estimation algorithm using pseudocovariance matrix," *IEEE Trans. Antennas Propagat.*, Vol. 53, No. 4, 1346–1351, 2005.
21. Abeida, H. and J.-P. Delmas, "MUSIC-like estimation of direction of arrival for noncircular sources," *IEEE Trans. Signal Processing*, Vol. 54, No. 7, 2678–2690, 2006.
22. Ye, Z. and C. Liu, "2-D DOA estimation in the presence of mutual coupling," *IEEE Trans. Antennas Propagat.*, Vol. 56, No. 10, 3150–3158, 2008.
23. Zhang, Y. and B. P. Ng, "MUSIC-like DOA estimation without estimating the number of sources," *IEEE Trans. Signal Processing*, Vol. 58, No. 3, 1668–1676, 2010.
24. Barabell, A., "Improving the resolution performance of eigenstructure-based direction-finding algorithms," *IEEE International Conference on Acoustics, Speech, and Signal Processing, ICASSP'83*, 336–339, 1983.
25. Rao, B. D. and K. V. S. Hari, "Performance analysis of Root-Music," *IEEE Trans. Acoust., Speech, Signal Processing*, Vol. 37, No. 12, 1939–1949, 1989.
26. Krim, H., P. Forster, and J. G. Proakis, "Operator approach to

performance analysis of root-MUSIC and root-min-norm," *IEEE Trans. Signal Processing*, Vol. 40, No. 7, 1687–1696, 1992.

27. Shan, T., M. Wax, and T. Kailath, "On spatial smoothing for direction-of-arrival estimation of coherent signals," *IEEE Trans. Acoust., Speech, Signal Processing*, Vol. 33, No. 4, 806–811, 1985.
28. Haber, F. and M. Zoltowski, "Spatial spectrum estimation in a coherent signal environment using an array in motion," *IEEE Trans. Antennas Propagat.*, Vol. 34, No. 3, 301–310, 1986.
29. Rao, B. D. and K. V. S. Hari, "Weighted subspace methods and spatial smoothing: Analysis and comparison," *IEEE Trans. Signal Processing*, Vol. 41, No. 2, 788–803, 1993.
30. Wang, H. and K. J. R. Liu, "2-D spatial smoothing for multipath coherent signal separation," *IEEE Trans. Aerosp. Electron. Syst.*, Vol. 34, No. 2, 391–405, 1998.
31. Li, F. and R. J. Vaccaro, "Sensitivity analysis of DOA estimation algorithms to sensor errors," *IEEE Trans. Aerosp. Electron. Syst.*, Vol. 28, No. 3, 708–717, 1992.
32. Ferreol, A., P. Larzabal, and M. Viberg, "On the resolution probability of MUSIC in presence of modeling errors," *IEEE Trans. Signal Processing*, Vol. 56, No. 5, 1945–1953, 2008.
33. Kaveh, M. and A. Barabell, "The statistical performance of the MUSIC and the minimum-norm algorithms in resolving plane waves in noise," *IEEE Trans. Acoust., Speech, Signal Processing*, Vol. 34, No. 2, 331–341, 1986.
34. Kaveh, M. and A. Barabell, "The statistical performance of the MUSIC and the minimum-norm algorithms in resolving plane waves in noise," *IEEE Trans. Acoust., Speech, Signal Processing*, Vol. 34, No. 3, 633–633, 1986.
35. Choi, J. and I. Song, "Asymptotic distribution of the MUSIC null spectrum," *IEEE Trans. Signal Processing*, Vol. 41, No. 2, 985–988, 1993.
36. Messer, H. and Y. Rockah, "On the eigenstructure of the signal-only tempo-spatial covariance matrix of broad-band sources using a circular array," *IEEE Trans. Acoust., Speech, Signal Processing*, Vol. 38, No. 3, 557–559, 1990.
37. Friedlander, B. and A. J. Weiss, "Direction finding using spatial smoothing with interpolated arrays," *IEEE Trans. Aerosp. Electron. Syst.*, Vol. 28, No. 2, 574–587, 1992.
38. Gardner, W. A., "Simplification of MUSIC and ESPRIT by exploitation of cyclostationarity," *Proceedings of the IEEE*, Vol. 76, No. 7, 845–847, 1988.

39. Stoica, P. and A. Nehorai, "Performance comparison of subspace rotation and MUSIC methods for direction estimation," *IEEE Trans. Signal Processing*, Vol. 39, No. 2, 446–453, 1991.
40. Yu, X. and K. M. Buckley, "Bias and variance of direction-of-arrival estimates from MUSIC, MIN-NORM, and FINE," *IEEE Trans. Signal Processing*, Vol. 42, No. 7, 1812–1816, 1994.
41. Yeh, C.-C., J.-H. Lee, and Y.-M. Chen, "Estimating two-dimensional angles of arrival in coherent source environment," *IEEE Trans. Acoust., Speech, Signal Processing*, Vol. 37, No. 1, 153–155, 1989.
42. Mathews, C. P. and M. D. Zoltowski, "Eigenstructure techniques for 2-D angle estimation with uniform circular arrays," *IEEE Trans. Signal Processing*, Vol. 42, No. 9, 2395–2407, 1994.
43. Wang, Y.-Y., L.-C. Lee, S.-J. Yang, and J.-T. Chen, "A tree structure one-dimensional based algorithm for estimating the two-dimensional direction of arrivals and its performance analysis," *IEEE Trans. Antennas Propagat.*, Vol. 56, No. 1, 178–188, 2008.
44. Wang, H. and K. J. R. Liu, "2-D spatial smoothing for multipath coherent signal separation," *IEEE Trans. Aerosp. Electron. Syst.*, Vol. 34, No. 2, 391–405, 1998.
45. Lei, Z. and T. J. Lim, "Estimation of directions of arrival of multipath signals in CDMA systems," *IEEE Trans. Commun.*, Vol. 48, No. 6, 1022–1028, 2000.
46. Chiang, C.-T. and A.-C. Chang, "DOA estimation in the asynchronous DS-CDMA system," *IEEE Trans. Antennas Propagat.*, Vol. 51, No. 1, 40–47, 2003.
47. Li, J., Z.-S. Liu, and P. Stoica, "3-D target feature extraction via interferometric SAR," *Radar, Sonar & Navigation, IET*, Vol. 144, No. 2, 71–80, 1997.
48. Kim, K.-T., S.-W. Kim, and H.-T. Kim, "Two-dimensional ISAR imaging using full polarisation and super-resolution processing techniques," *Radar, Sonar & Navigation, IET*, Vol. 145, No. 4, 240–246, 1998.
49. Kim, K.-T., D.-K. Seo, and H.-T. Kim, "Radar target identification using one-dimensional scattering centres," *Radar, Sonar & Navigation, IET*, Vol. 148, No. 5, 285–296, 2001.
50. Miwa, T. and I. Arai, "Super-resolution imaging for point reflectors near transmitting and receiving array," *IEEE Trans. Antennas Propagat.*, Vol. 52, No. 1, 220–229, 2004.
51. Quinquis, A., E. Radoi, and F. C. Totir, "Some radar imagery results using Super-resolution techniques," *IEEE Trans. Antennas*

Propagat., Vol. 52, No. 5, 1230–1244, 2004.

52. Gini, F., F. Lombardini, and M. Montanari, "Layover solution in multibaseline SAR interferometry," *IEEE Trans. Aerosp. Electron. Syst.*, Vol. 38, No. 4, 1344–1356, 2002.
53. Urazghildiiev, I., R. Ragnarsson, and A. Rydberg, "High-resolution estimation of ranges using multiple-frequency CW radar," *IEEE Trans. Intell. Transport. Syst.*, Vol. 8, No. 2, 332–339, 2007.
54. Secmen, M. and G. Turhan-Sayan, "Radar target classification method with reduced aspect dependency and improved noise performance using multiple signal classification algorithm," *Radar, Sonar & Navigation, IET*, Vol. 3, No. 6, 583–595, 2009.
55. Li, L., W. Zhang, and F. Li, "A novel autofocusing approach for real-time through-wall imaging under unknown wall characteristics," *IEEE Trans. Geosci. Remote Sensing*, Vol. 48, No. 1, 423–431, 2010.
56. Zhang, W., A. Hoorfar, and L. Li, "Through-the-wall target localization with time reversal music method," *Progress In Electromagnetics Research*, Vol. 106, 75–89, 2010.
57. Lazarov, A. D., "Iterative MMSE method and recurrent Kalman procedure for ISAR imaging reconstruction," *IEEE Trans. Aerosp. Electron. Syst.*, Vol. 37, 1432–1441, 2001.
58. Li, L., W. Zhang, and F. Li, "Tomographic reconstruction using the distorted rytov iterative method with phaseless data," *IEEE Geoscience and Remote Sensing Letters*, Vol. 5, 479–483, 2008.
59. Zhang, W., A. Hoorfar, and C. Thajudeen, "Polarimetric through-the-wall imaging," *2010 URSI International Symposium on Electromagnetic Theory (EMTS)*, 471–474, Berlin, Germany, 2010.
60. Zhang, W., L. Li, and F. Li, "Multifrequency imaging from intensity-only data using the phaseless data distorted Rytov iterative method," *IEEE Trans. Antennas Propagat.*, Vol. 53, 290–294, 2009.
61. Hudson, J. E., *Adaptive Array Principle*, Peter Peregrinus Ltd., London, UK, 1981.
62. Wilkinson, J. H., *The Algebraic Eigenvalue Problem*, Oxford University Press, Inc., New York, USA, 1965.